Journal of
Materials Chemistry C

PAPER

View Article Online
View Journal | View Issue

Cite this: J. Mater. Chem. C, 2016, 4, 1295

Multilayer MoS_2 growth by metal and metal oxide sulfurization†

M. H. Heyne,*[abc] D. Chiappe,[ab] J. Meersschaut,[b] T. Nuytten,[b] T. Conard,[b] H. Bender,[b] C. Huyghebaert,[b] I. P. Radu,[b] M. Caymax,[b] J.-F. de Marneffe,[b] E. C. Neyts[c] and S. De Gendt[ab]

Received 2nd December 2015,
Accepted 4th January 2016

DOI: 10.1039/c5tc04063a

www.rsc.org/MaterialsC

We investigated the deposition of MoS_2 multilayers on large area substrates. The pre-deposition of metal or metal oxide with subsequent sulfurization is a promising technique to achieve layered films. We distinguish a different reaction behavior in metal oxide and metallic films and investigate the effect of the temperature, the H_2S/H_2 gas mixture composition, and the role of the underlying substrate on the material quality. The results of the experiments suggest a MoS_2 growth mechanism consisting of two subsequent process steps. At first, the reaction of the sulfur precursor with the metal or metal oxide occurs, requiring higher temperatures in the case of metallic film compared to metal oxide. At this stage, the basal planes assemble towards the diffusion direction of the reaction educts and products. After the sulfurization reaction, the material recrystallizes and the basal planes rearrange parallel to the substrate to minimize the surface energy. Therefore, substrates with low roughness show basal plane assembly parallel to the substrate. These results indicate that the substrate character has a significant impact on the assembly of low dimensional MoS_2 films.

Introduction

Transition-metal dichalcogenides (TMD) such as MoS_2 or WS_2 are interesting materials for future transistor applications, but their large-area deposition is challenging. The first transistor devices based on TMDs were demonstrated on mechanically exfoliated flakes.[1,2] The mechanical exfoliation allows only the deposition of sheets up to a few μm^2 size, which makes this process inappropriate for high device densities on large areas. In addition, exfoliated flakes which are considered as best material quality at this juncture, show spatial variations in their properties.[3–5] TMD films have been deposited by chemical vapor deposition[6–8] on substrates up to a few cm^2. This deposition can be achieved by the vaporization of solid MoO_3 and S in a furnace under inert carrier gas flow. However, this technique is very sensitive to the amount of the precursor, the carrier gas flow in the furnace, and the substrate temperature itself, and therefore it is difficult to scale to larger substrate dimensions. To decrease the vaporization influence of the metal precursor, it is possible to pre-deposit a transition-metal (TM) or transition-metal oxide (TMO) on a substrate with subsequent sulfurization from a S source.[9–13] The homogeneous S supply can also be achieved by using a gaseous precursor such as H_2S.[14–21] The present paper elucidates the mechanisms of MoS_2 multilayer synthesis by the sulfurization technique. The influence of the process temperature, annealing time, and ramp rate is studied, as well as the nature of the pre-deposited layers MoO_3, metallic Mo, and the nature of the substrate. The synthesis ambient was compared for mixtures of H_2S/H_2 *vs.* pure H_2S. The grown films were characterized by various optical, morphological, and structural techniques. The highest quality MX_2 films have been only demonstrated on atomically flat substrates such as graphene or other exfoliated MX_2 substrate layers,[22,23] but the deposition on amorphous substrates is desirable due to their availability for large area substrates such as 300 mm wafer. This paper establishes guidelines for the synthesis of horizontally aligned transition-metal dichalcogenide multilayer thin films on SiO_2.

Experimental

TM and TMO deposition

The Mo-based TM and TMO films were prepared by physical vapor deposition on top of thermal or native silicon oxide substrates. To deposit TMO, oxygen was added as reactive component in the PVD deposition. We studied a thick 5 nm Mo-film on 270 nm wet thermal silicon oxide (stack A), a thin

[a] KU Leuven, University of Leuven, Department of Chemistry, Celestijnenlaan 200f - box 2404, 3001 Leuven, Belgium. E-mail: markus.heyne@chem.kuleuven.be
[b] IMEC, Kapeldreef 75, 3001 Leuven, Belgium
[c] University of Antwerp, Department Chemistry, Universiteitsplein 1, 2610 Antwerp-Wilrijk, Belgium

† Electronic supplementary information (ESI) available. See DOI: 10.1039/c5tc04063a

2 nm Mo-film on 270 nm wet thermal silicon oxide (stack B), and a 5 nm reactively sputtered MoO_x on thin native silicon oxide (stack C).

Sulfurization of the TM and TMO films

The samples were sulfurized *ex situ* in a 6 inch rapid thermal processing (RTP) chamber ANNEALSYS-ONE-150 equipped with H_2 and H_2S gas supply. For this purpose, the samples were placed on top of a SiC-coated graphite susceptor in the annealing chamber. The chamber was pumped to vacuum and then the temperature was increased to the target temperature 400 °C, 600 °C, or 800 °C. The gas mixture of 10% or 100% H_2S in H_2 was injected until the pressure reached 100 mbar and kept under static conditions for the process duration of 5 min to 30 min. Afterwards, the heating was stopped, the chamber was cooled down and pumped to vacuum again for 20 min.

Characterization of the films

The films were analyzed by Rutherford backscattering spectrometry (RBS) to determine the amount of Mo and S after the sulfurization. The accelerator at imec is a 6SDH Pelletron accelerator from the National Electrostatics Corporation (NEC). To this end, a He-beam with an energy of 1.523 MeV and beam currents of 20 nA to 40 nA were used. The scattering angle was 170° and the tilt angle was 11°. The used goniometer is described in literature.[24] Before the measurement, the incident beam was calibrated to a reference material of an AlW/TiN/Si substrate. A representative spectra of MoS_2 can be found in Fig. 1. Raman spectroscopy with a LabRAM HR tool was used to characterized the films' quality using an excitation wavelength of 532 nm and a grating of 1800 grooves per mm, yielding a theoretical resolution of 0.3 cm^{-1}. A scanning electron microscope (SEM) FEI Nova 200 was used to investigate the surface morphology. Transmission electron microscopy (TEM) cross-section images were obtained with a FEI Tecnai F30 ST at 200 kV and plan-view images with Titan^3 60–300 at 60 kV. The surface roughness was determined by an atomic force microscope (AFM) Dimension-Icon PT. Angle-resolved X-ray photoelectron spectra (ARXPS) were measured with a Theta 300 system from ThermoInstruments. X-ray diffraction characterization was done with PANALYTICAL X'PERT.

Results

Part I: growth parameter study

Analysis of the pre-deposited material. TM and TMO films were deposited on 270 nm wet thermal silicon oxide substrates. The 5 nm (stack A) and 2 nm (stack B) metallic films oxidized partially or fully as soon as they were exposed to ambient. A third test specimen with 5 nm MoO_x (stack C) on thin native silicon oxide was prepared by reactive sputtering. To determine the level of surface oxidation, stacks A, B, and C were analyzed by angle-resolved X-ray photoelectron spectroscopy (ARXPS). Information about the oxidation state was gained from the energy shift of the Mo 3d peak.[25,26] Fig. 2 shows the all-integrated, normalized Mo 3d peaks in the XPS spectra for the three different stacks and the angle-resolved Mo 3d peak for stack A.

At 78°, the spectra for all three samples overlap, showing no metallic contribution, therefore indicating that all samples, TM and TMO, have an oxidized surface. By probing deeper under the surface, *i.e.* 21° angle, it was found that only stack A shows a peak at the lower binding energy around 228 eV. The spectra for stacks B and C appear similar and they do not show this peak at low binding energy.

Sulfurization process. Starting from a typical 10% H_2S/H_2 mixture as it is used in the MoS_2 catalyst preparation,[27] the temperature window between 400 °C and 800 °C was investigated. Afterwards, the influence of the H_2 addition on the deposited film was explored. We subsequently tested the reaction time dependence and finally compared the influence of the underlying film on the growth conditions.

Influence of the processing temperature. The sulfurization of the stacks A, B, and C was carried out at temperatures of 400 °C, 600 °C, and 800 °C. The chamber was heated in vacuum until the target temperature was reached, and subsequently the H_2S gas was introduced and kept in the chamber for 5 min under static conditions. Afterwards, the chamber was evacuated and cooled down passively. The samples were characterized by Rutherford

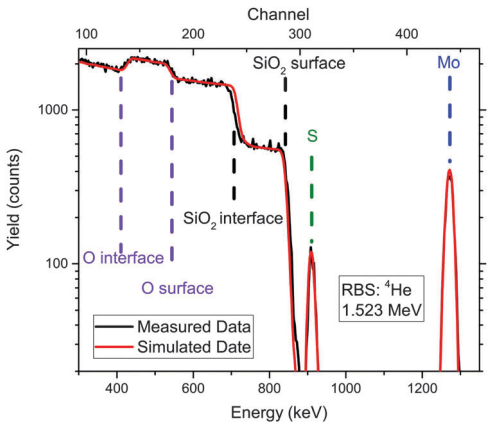

Fig. 1 RBS spectrum of a MoS_2 film sulfurized from a stack of 2 nm Mo/270 nm SiO_2/Si substrate.

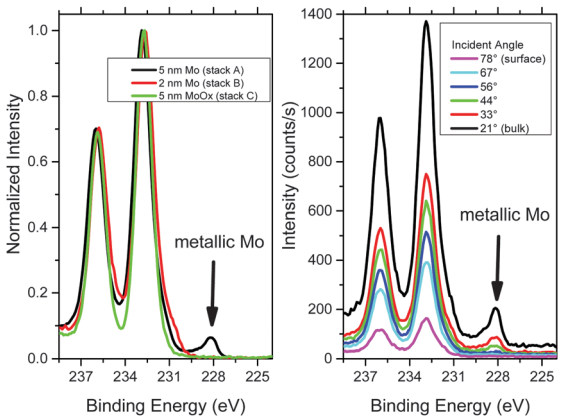

Fig. 2 ARXPS on stacks A, B, and C before sulfurization showing oxidation of the layers and buried metallic Mo on stack A.

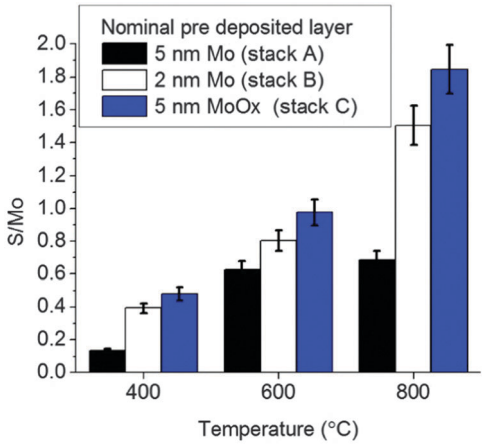

Fig. 3 S/Mo ratio of different stacks after 5 min sulfurization at different temperatures in a 10% H_2S/H_2 mixture as determined by RBS.

backscattering spectrometry (RBS) and the ratio of the atomic areal density of S and Mo was calculated. The resulting S/Mo ratios are shown in Fig. 3.

After sulfurization at 400 °C, the S/Mo ratio did not exceed 0.5 in any of the samples, increasing to the range 0.6–1.0 for the 600 °C-treated samples and up to a range 0.6–1.9 for the 800 °C-treated samples. At 800 °C, the sulfurization in stack C was higher than in stack B at 800 °C, while in contrast, stack A could not be fully sulfurized in the H_2S/H_2 mixture even at 800 °C within the 5 min processing time in the H_2S/H_2 mixture. In the next paragraph, the influence of the hydrogen fraction in the gas mixture is described.

Influence of the hydrogen fraction in the sulfurization process. Samples of stack A, B, and C were heated to 600 °C and the 10% H_2S/H_2 mixture or pure 100% H_2S was injected in the chamber and kept under static conditions for five minutes. Afterwards, the samples were characterized by RBS and the S/Mo ratio was calculated. Stack A had a relatively low S/Mo ratio of below 0.8 for both annealing conditions (Fig. 4). In contrast, stacks B and C showed significant differences with the 10% mixture showing a S/Mo ratio of only 0.8 to 1.0 after 5 min, whereas the pure H_2S resulted in a ratio of about 2.

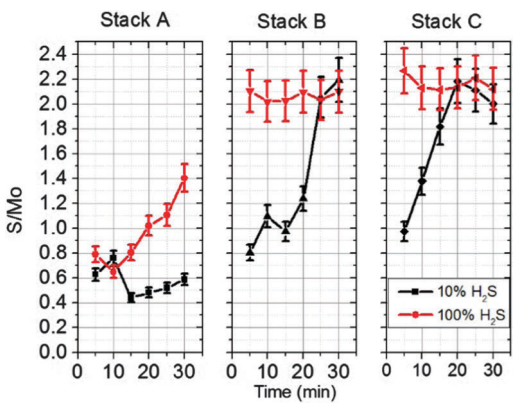

Fig. 4 S/Mo ratios as calculated from the RBS atomic areal density, for sulfurization of TM and TMO at 600 °C in H_2-diluted and pure H_2S.

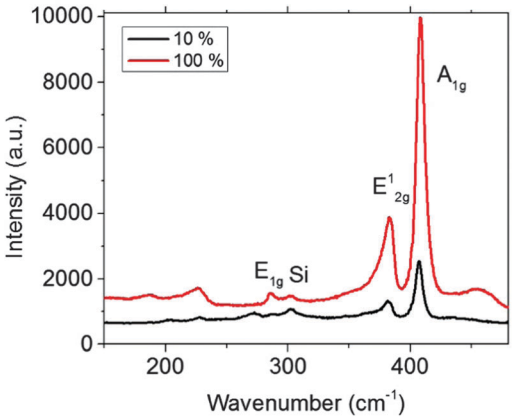

Fig. 5 Raman spectra of a stack B sample annealed for 5 min at 600 °C in H_2-diluted and pure H_2S.

The Raman spectra taken after sulfurization in 10% and 100% H_2S are depicted in Fig. 5. The samples annealed in pure H_2S showed higher MoS_2-related peak intensity than in diluted H_2S, further confirming the results from RBS.

We also investigated the time-dependence for TM/TMO film conversion. To this end, the stacks A, B, and C were sulfurized either in 10% or 100% H_2S for different times, and the S/Mo ratio was determined by RBS as shown in Fig. 4.

Stack A of the 5 nm Mo shows a moderate time-dependency of the sulfurization under pure H_2S, although not reaching the target value of S/Mo = 2, while in the case of H_2 dilution, the sulfurization is only marginally dependent on processing time. In contrast, stacks B and C show significant time-dependent sulfurization under H_2 dilution and even immediate stoichiometric sulfurization already after 5 minutes processing time in the case of pure H_2S. The sulfurization under H_2 dilution was slower than in pure H_2S in all cases studied.

Annealing with optimized conditions. Based on the fact that stack A required a sulfurization temperature of 800 °C and pure H_2S gas for 30 min to reach a S/Mo close to 2, these conditions were applied to different initial thicknesses of deposited Mo on SiO_2 and characterized by RBS after the sulfurization process. Fig. 6 shows that the S/Mo ratio as calculated from Mo and S amount is between 1.8 and 2 and thus, stoichiometric. Layers of initially 5 nm metallic Mo resulted in approximately 25 nm MoS_2 films.

Part II: MoS_2 plane orientation

Effect of ramp rate and interlayer oxide. The surface topology of the stacks B and C was compared by scanning electron microscopy (SEM) and atomic force microscopy (AFM) after annealing without H_2S and after the sulfurization process with 100% H_2S. The results are illustrated in Table 1, Fig. S1 and S2 (ESI†).

The as-deposited metal and metal-oxide films had an initial RMS roughness of 0.3 nm to 0.4 nm. After annealing in vacuum, the samples of stack B roughened. Annealing in 100% H_2S increased the surface roughness even more. The arithmetic roughness parameter R_a of the H_2S annealed stack B was R_a = 2 nm.

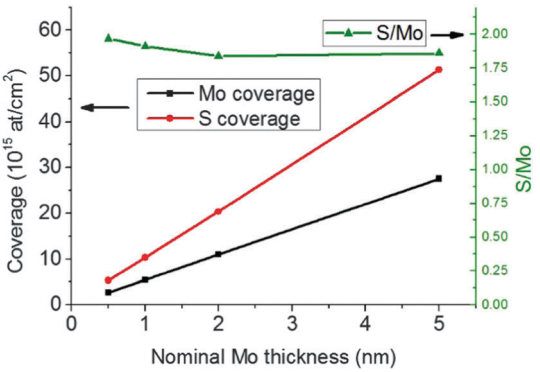

Fig. 6 Coverage of Mo and S and the S/Mo ratio after 800 °C sulfurization in 100% H_2S for 30 min as a function of the initial sputtered Mo thickness determined by RBS.

Table 1 Comparison of the surface roughness of different stacks after sulfurization at 800 °C in 100% H_2S for 30 min. The scanned area was 2×2 μm^2

	B	C
Pristine	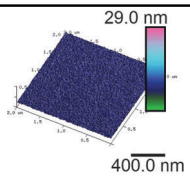	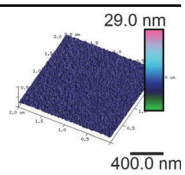
After H_2S annealing	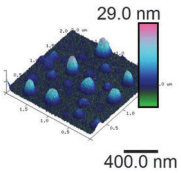	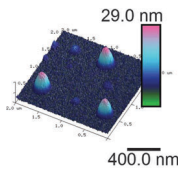

In contrast, stack C with the TMO on the native oxide showed less roughening than stack B in vacuum as well as in H_2S. The roughness of stack C was only R_a = 1.5 nm. Hence, the samples with the wet silicon oxide underneath roughened to a larger extent than the samples grown on native silicon oxide.

A smooth surface is important for potential integration of planar electronic devices. To investigate this, the samples of stack B and C were measured before and after the sulfurization process.

Significant roughening can be seen after the MoS_2 synthesis process on both sample surfaces, with hillocks appearing on the surface. The sulfurized stack B showed a larger density of these hillocks than stack C, and these bumps were higher than 20 nm after sulfurization. The TEM image in Fig. 7 shows that a delamination occurred at the interface between MoS_2 and SiO_2 substrate. Stack B showed more delamination sites than stack C and hence, MoS_2 on wet thermal oxide formed more hillocks than on native SiO_2.

Underlying substrate. The role of the underlying substrate on the basal plane arrangement will be studied in this section. To this end, stacks B and C were sulfurized at 600 °C in pure H_2S. The TEM cross section images are shown in Table 2.

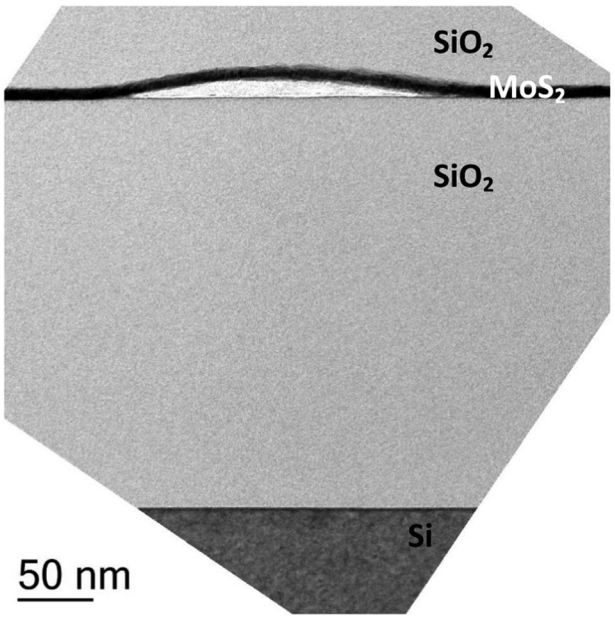

Fig. 7 TEM image showing delamination of the MoS_2 film (dark) from the SiO_2 substrate (bright).

Stack B reveals two preferential layer orientations after the 600 °C sulfurization. While the surface layers appear rather horizontal, the bulk material is oriented more vertical to the substrate. The layered structure can be seen in the whole film and thus, the H_2S precursor is diffusing throughout the whole film, even at 600 °C.

However, stack C revealed a horizontally layered structure over the full thickness after the 600 °C sulfurization. At the same time, the interface oxide of 3–4 nm was thicker than the usual native oxide of around 1 nm, meaning that the oxide thickness has increased during the high temperature step. A similar horizontal assembling like in stack B could only be reached at a higher temperature of 800 °C, leading us to conclude that the interfacial oxide thickness and substrate type result in an interplay with different sulfurization temperatures to different basal plane assemblies. On thin silicon oxide, the horizontal alignment took place at lower temperature than on thick SiO_2.

The lattice spacing derived from the cross-section TEM images in Table 2 are between 0.60 nm and 0.65 nm. The accuracy is low due to the thin layer and irregular oriented planes. The range of the spacing correspond to the expected 0.61 nm for the stoichiometric MoS_2 in 2H phase.

Part III: MoS_2 quality

Hydrophobicity and crystallinity. Ideal horizontally layered MoS_2 is expected to be hydrophobic due to the sulfur surface termination. In contrast, material exposing many edges to the top is expected to be hydrophilic due to the reactive nature of the edges. Table 3 shows a contact angle of 93° for the MoS_2 deposited at 800 °C, which demonstrates the hydrophobic character as compared to SiO_2 or MoO_3 surface. After the sulfurization under the optimized conditions of 800 °C for

Table 2 TEM images of different stack sulfurized in 100% H_2S

Sulfurized stack B at 600 °C in H_2S: MoS_2 on thick SiO_2	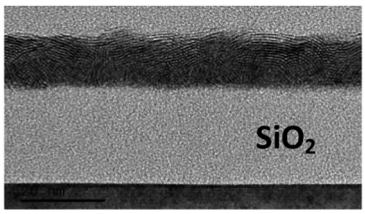
Sulfurized stack C at 600 °C in H_2S: MoS_2 on thin SiO_2	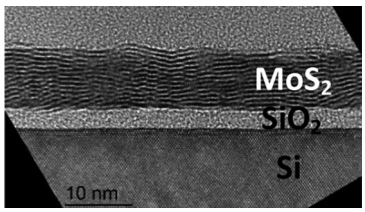
Sulfurized Stack B at 800 °C in H_2S: MoS_2 on thick SiO_2	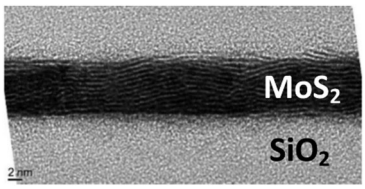

Table 3 Contact angles on a SiO_2 substrate, a molybdenum oxide sample, and a 800 °C sulfurized MoS_2 sample

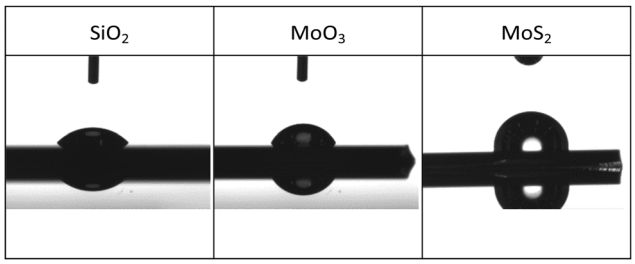

30 min in 100% H_2S, the sample was characterized by glancing-incidence XRD (GIXRD). The film showed the characteristic MoS_2(002) peak around 14.3° as can be seen from Fig. 8.[28,29]

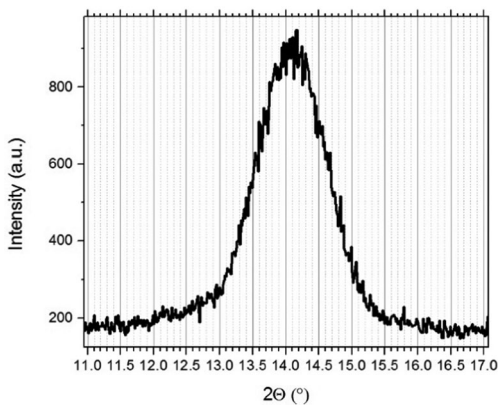

Fig. 8 GIXRD spectrum of the MoS_2(002)-related peak synthesized from stack C at 800 °C in 100% H_2S during 30 min.

Plan-view TEM images. Besides the qualitative and quantitative analysis of the MoS_2 crystal structure, the determination of the crystal grain size is essential since grain boundaries act as defects for charge transport, negatively impacting the mobility of these materials. To determine the grain size, the MoS_2 had to be transferred to a thin e-beam-transparent membrane suitable for TEM imaging. To this purpose, the samples were immersed in water and the films peeled off from the substrates.[30]

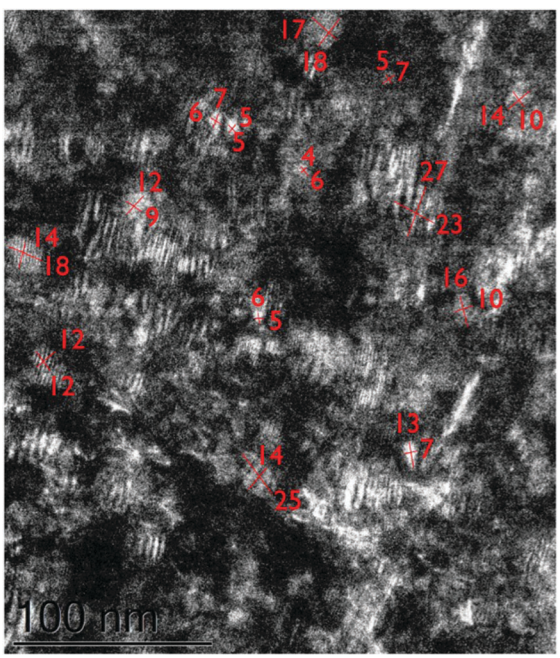

Fig. 9 TEM image from stack C annealed at 800 °C in dark field mode indicating crystal sizes in the 10–25 nm range.

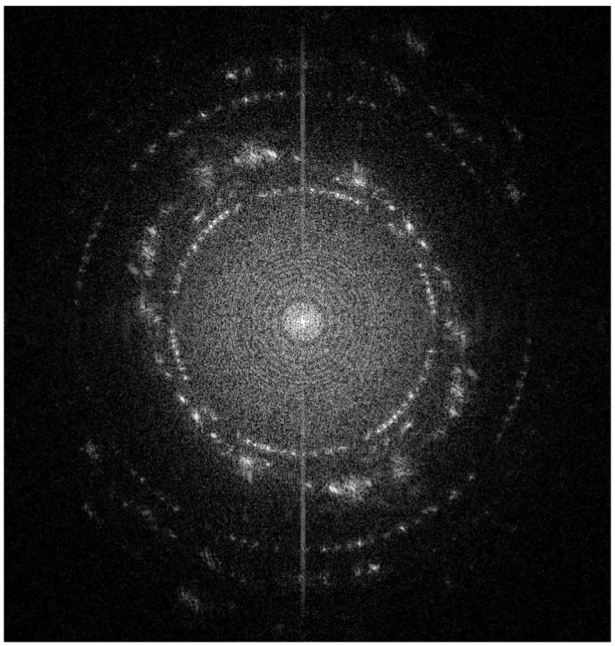

Fig. 10 FFT of a plan-view image of stack C annealed at 800 °C for 30 min.

Subsequently the films could be transferred to a thin Si_3N_4 membrane which is nearly transparent for the electron beam. The image in Fig. 9 shows grain sizes in the 10 to 25 nm range. Due to varying orientation of the crystal planes as can be seen on the cross-sectional TEM images in Table 2 and the electron scattering on the underlying Si_3N_4, an atomic pattern was barely observable on the plan-view images. Electron diffraction and Fast-Fourier transformed images in Fig. 10 show that the MoS_2 is nearly oriented along [0001] with random in-plane orientation of the grains and probably fully in the 2H phase.

Surface chemical analysis. The XPS spectra of the Mo 3d peak are depicted in Fig. 11. After the sulfurization at 800 °C, a peak shift to lower binding energies characteristic for MoS_2, can be seen. The peak appearing around 227 eV is related to the S 2s region.

Photoluminescence. A quality feature of thin layers of TMD materials is the photoluminescence (PL) appearing due to the direct bandgap transition.[31–34] In Fig. 12 the intensity change in the direct excitonic transitions A1 and B1 for different starting Mo thicknesses is plotted, showing a higher PL for thinner sulfurized layers. This evidences the band gap opening towards thinner layers and proves an acceptable material quality.

Discussion

Part I: growth parameter study

Analysis of deposited material. Only the thick stack A shows a Mo photoelectron peak at lower binding energy indicating a metallic contribution. Together with the angle-resolved measurements, this revealed that the surface was oxidized in air and only the bottom part of the layer at the interface with

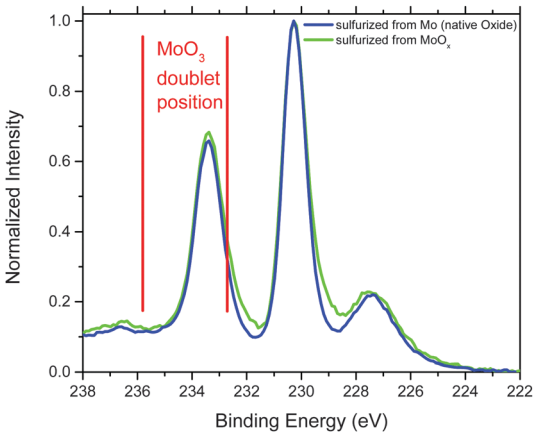

Fig. 11 Mo 3d peak in XPS spectra for pristine samples and 800 °C in 100% H_2S sulfurized samples.

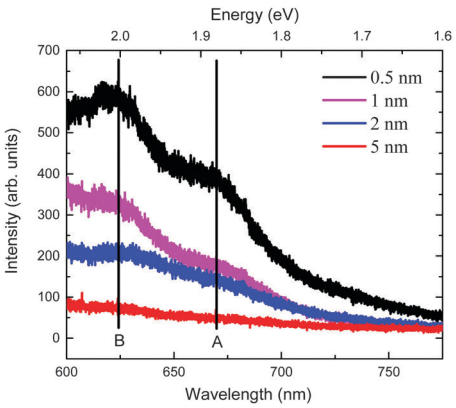

Fig. 12 Photoluminescence measured on samples synthesized at 800 °C in 100% H_2S for 30 min from different starting thicknesses.

the substrate was metallic. In contrast, similar spectra for stacks B and C indicated that the chemical state was uniform throughout the entire film, *i.e.* stack B oxidized completely in air. The formed oxides appear in the XPS as a doublet at relatively high binding energy close to the one of MoO_3 at 233.1 eV. This is why the synthetic as well as the native oxides can be assumed to have the trioxide structure. Thus, the TMO of stack B and C was comparable and differed mainly in the underlayer, being a thick thermal oxide in stack B and a thin native oxide in stack C.

The root-mean-square (RMS) roughness in the range of 0.2 to 0.3 nm was slightly higher than expected on a polished Si surface (0.1 nm), but still reasonable for an oxidized substrate covered with a PVD metallic film. The stack roughness of 0.3 nm was acceptable taking into account a MoS_2 monolayer thickness of 0.7 nm.

Sulfurization process optimization

Temperature. Higher temperature resulted in a higher sulfurization degree. Stacks B and C could be sulfurized almost stoichiometrically at 800 °C in the H_2S/H_2 mixture, while lower temperatures only resulted in a partial sulfurization.

Stack A containing the metallic Mo could not be sulfurized in the mixture, not even at high temperature.

The absolute sulfur content in the sulfurized stack A was compared with the Mo amount in stacks B and C. Stack B represented a metallic film being completely oxidized in air. Thus, the thicker stack A could be assumed to be a double stack of native top Mo-oxide comparable to stack B and C and a metallic part underneath. The ratio of the amount of sulfur to the amount of oxidized Mo was 0.2, 1.4, and 1.6 for 400 °C, 600 °C, and 800 °C, respectively. This is comparable to the S/Mo ratios for stacks B and C, indicating that at 600 °C mainly the oxidized part was sulfurized, but not the metallic part. From these observations, we conclude that the sulfurization of MoO_3 proceeds at lower temperature than the sulfurization of metallic Mo.

The involved reactions are the following:

$$MoO_{3(g)} + 3H_2S_{(g)} \rightleftharpoons MoS_{2(s)} + 3H_2O_{(g)} + S_{(s)} \quad (I)$$

$$Mo_{(s)} + 2H_2S_{(g)} \rightleftharpoons MoS_{2(s)} + 2H_{2(g)} \quad (II)$$

The software module reaction equations from the package HSC Chemistry was used to calculate the change in Gibbs free energy for the reactions (I) and (II) by simply calculating the differences in enthalpy and entropy taken from a database. The results in the temperature range from 0 °C to 1000 °C are depicted in Fig. 13. The Gibbs free energy is negative over a large temperature range and thus, both reactions should proceed spontaneously. Reaction (II) has a higher Gibbs free energy than reaction (I) in the high temperature range above 200 °C. Hence, the sulfurization of metallic Mo requires higher temperature or longer annealing time than the sulfurization of MoO_3. This was confirmed by our observation that the metal-containing film remained non-stoichiometric, even after a long sulfurization processes.

The data also indicated that stack C was sulfurized to a higher degree than stack B. This shows that their behavior was slightly different despite their similar chemical nature as the XPS data have shown. The major difference in these samples was the substrate, *i.e.* thin (stack C) or thick (stack B) silicon oxide underneath. In case of the thin oxide, reaction byproducts could diffuse easier through the thin native oxide than through the thick native oxide and scavenged by the silicon underneath.

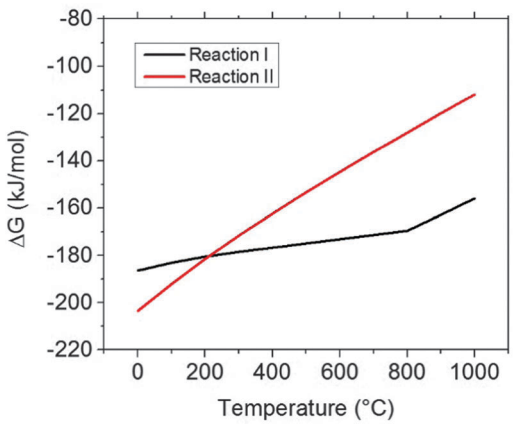

Fig. 13 Change in Gibbs free energy for reaction (I) and (II) as a function of temperature.

Partial Pressure and Time. Hydrogen is reported to reduce MoS_2 at temperatures above 500 °C,[35] although this reaction is energetically unfavorable with ΔG = +200 kJ mol^{-1}, H_2 was excluded from the process gasses by switching to pure H_2S. As demonstrated, the sulfurization with pure H_2S was faster compared to the sulfurization with the 10% mixture, indicating that hydrogen must have hampered the sulfurization reaction. This can be attributed to different mechanisms.[36] We assume that the sulfurization reaction for either oxidized or metallic Mo occurs alongside reactions (I) and (II), respectively.

Reaction (I) has a change in Gibbs free energy of −173 kJ mol^{-1}, whereas reaction (II) has −145 kJ mol^{-1}. Thus, both reaction are exergonic and proceed spontaneously. If hydrogen is added to reaction (II), the concentration on the product side will increase and will slow down the reaction. While the mixture with hydrogen does not show any time-dependence in Fig. 4, the pure H_2S showed an increasing sulfurization degree with time, although it did not reach stoichiometry in this time-frame at this temperature. Thus, hydrogen plays a crucial role in the sulfurization of the samples with the metallic core.

In contrast, stacks B and C showed a time-dependent S/Mo ratio in case of the H_2S/H_2 mixture, but a constant, stoichiometric ratio in case of the pure H_2S. In reaction (I), no hydrogen is involved, meaning that the faster process can only be explained by the increase of the H_2S partial pressure from 10 mbar to 100 mbar. The higher H_2S amount induced a faster sulfurization while the hydrogen did not influence the chemical reaction.

From the previous experiments, it can be concluded that a high sulfurization temperature, longer sulfurization time, and higher H_2S partial pressure resulted in enhanced material quality. For metallic films the reaction kinetics were influence by the hydrogen partial pressure. Although thin films of stacks B and C could be sulfurized at a temperature of 600 °C, the sulfurization of thicker films like in stack A was not possible within 30 min annealing time. Therefore, the sulfurization temperature was further increased to 800 °C in order to facilitate a full sulfurization of the thicker films and to ensure the full conversion of metallic Mo.

To verify the full sulfurization, starting layers of different thicknesses were prepared and annealed under similar conditions. The Mo and S areal densities show a linear trend proportional to the initially deposited Mo thickness. This confirms that the higher temperature is necessary in order to allow the full sulfurization of thicker, metallic layers as well.

Part II: MoS_2 plane orientation

After optimization of the annealing conditions for metallic and metal-oxide-based layers, the deposited films were characterized to gain an understanding of the mechanisms which are driving the sulfurization. In the ideal case, two-dimensional films are entirely flat. The surface topology of our samples was characterized by SEM and AFM after annealing, showing different topographical

roughness for the different conditions. Whereas stacks A and B revealed surface roughening after annealing, stack C showed better wetting on the underlayer, and this effect appeared after annealing in vacuum as well as in H_2S environment. However, the latter showed stronger roughening, which indicates that the roughening is related to both the substrate and the environment as the images in Table 1 demonstrate.

The interface material between the MoS_2 film and the substrate was in all cases SiO_2, thus the surface energy of the two substrates can be assumed to be similar. However, the alignment of the MoS_2 basal planes differed between the samples with thick and thin SiO_2. The MoS_2 films on the thick wet-grown SiO_2 show macroscopically rough surface after annealing, whereas the MoS_2 films on the thin SiO_2 had a conformal surface as judged from the SEM images. A possible explanation is the formation and release or consumption of reaction byproducts. The sulfurization reactions release gaseous products which is H_2O in reaction (I) and H_2 in reaction (II). The deposition process occurring in different steps. Initially, the H_2S approaches the surfaces and the reaction starts there. Subsequently the H_2S needs to diffuse through the layers to react deeper into the sublayers. During this reaction, gaseous products will be formed which have to leave the film again. In case of metallic layers, this formed compound is H_2 which is small enough to easily escape towards the surface. However, the sulfurization of oxide results in H_2O formation which cannot easily escape the surface through the MoS_2, but can only slowly diffuse through the SiO_2 substrate.[37–39] If the diffusion at 700 °C was to slow, the H_2O might have accumulated at the MoS_2/substrate interface and lifted of the film which resulted in rough topology on the MoS_2 on thick silicon oxide or even delamination of the films. In the case of very thin 1.2 nm oxide, the H_2O could diffuse with lower activation energy through the thin barrier and oxidize the silicon underneath. Hence, the substrate may have acted as a scavenger for the reaction products of the sulfurization and the roughness of the layers and simultaneously their horizontal arrangement could be improved.

The roughness was induced by the hillocks on the sample surface and by the MoS_2 film itself. However, the surface images showed that the microroughness was superimposed to the hillocks which formed during the delamination of the MoS_2 films from the SiO_2 substrates.

The R_a determined as the arithmetic average from the absolute values reveals another difference between the samples. The sulfurized stack B showed a higher roughness of around 2 nm, whereas the TMO sulfurized stack C showed a roughness of 1.5 nm. The scavenged water or oxygen in the Si underneath might prevent the outgassing of water to the film surface and, as such, the chemical reaction is completed faster in stack C and it favors the plane alignment horizontal to the interface in a given reaction time. Stack B with the thicker oxide scavenges less water and thus the reaction takes longer before the planes realign.

Based on these observations, we conclude that the annealing on a thick SiO_2 layer already introduced roughness in vacuum by dewetting.[40] A H_2S flow during this annealing further increased this effect by releasing reaction byproducts. The basal planes were more horizontal when an underlying reservoir area for collecting reaction products was provided.

Part III: MoS_2 quality

Hydrophobicity. The surface wetting by water gives indications on the material quality. The wetting angle as well as the TEM observation of the 800 °C annealed sample are in agreement with results from literature,[37] revealing the hydrophobic nature of the surface which is correlated to the growth temperature and thus also with the MoS_2 structure.[41] As shown in the previous sections, material grown at low temperature which might be only partially sulfurized and did not go through the crystallization process yet, tends to form random structures oriented to the reactants' diffusion direction. This results in the exposure of many edge sites at the surface leading to a high surface energy and thus, a more hydrophilic behavior. In contrast, higher temperature favors the crystallization resulting in horizontal planes in which the edge exposure is decreased and hence results in low-energy, hydrophobic surfaces. This observation also confirms the improved quality of the material from the high temperature growth.

Crystal morphology. Comparing the assembly of the basal planes, the 600 °C sulfurization on thin native silicon oxide resulted in preferential horizontal arrangement of the basal planes. In contrast, layers on thick SiO_2 tend to form relatively rough films with random orientation. The chemical reaction to MoS_2 is faster and more time is given to the recrystallization process when using 30 min processing time. During the crystallization, the basal planes orient in a way to reduce their surface energy. Hence, on perfectly flat substrates such as native or thermally grown SiO_2, the basal planes will assemble parallel to the substrates and the following MoS_2 planes will orient in alignment with the basal planes.[42] Similar behavior is predicted for other flat substrates which could take up H_2O in a high temperature process or which are permeable for byproducts of the sulfurization reaction.

Comparing the sulfurization between a fully oxidized layer and a partially oxidized layer with metallic components, the oxidized films resulted in better film quality at lower temperature. Since the metallic layer needs a higher temperature and is more densely packed, the MoS_2 grown from metallic material suffers from the slow pace of material transport. The H_2S molecules need to diffuse through the metallic layer and induce an additional volume expansion of a factor of 4 which leads to mass transport and distort the structure itself. In contrast, the 5 nm MoO_3 layers are found to expand only by about a factor of 1.6 as is shown in Table 2. The observations from stack A confirm this. The TEM images of the thicker sulfurized stacks showed horizontally oriented crystals on the top. This top structure was directly sulfurized from the native oxide, which proceeds fast and efficient even at the relatively low temperature of 600 °C. However, the incompletely sulfurized bulk was vertically layered. This observation suggested that the TMD layered structure orient towards the diffusion direction of the gaseous reaction source material and products. Only after the reaction has finished and no more reactants force the plane

direction, the crystallization process takes place and the planes realign according to the interface with the underlying material. This confirms earlier reports exhibiting relatively random MoS_2 orientation on rough and thick SiO_2.[43–47]

Surface chemical state. The XPS spectra of the as-deposited metal-oxide and metal films can be interpreted mainly as MoO_3 and MoO_3/metallic layer, respectively. The NIST database reports the Mo 3d5/2 doublet for MoO_3 around 232.5 eV[25] and the metallic Mo peak is located at 228 eV.[48] In contrast, MoO_2 is reported around 229.3 eV and could not be clearly identified in the MoO_x layers. In the sulfurized MoS_2 films, the relatively high binding energy of the Mo 3d doublet of MoS_2 suggests a mainly 2H polytype since the 1T polytype is usually located at lower binding energies.[49] This is also in agreement with the 2H lattice distances measured from the TEM cross-sections.[50,51] The 2H polytype is expected to be semiconducting, whereas the 1T is a more metallic phase making the material promising for integration as a transistor channel. The absence of MoO_3-related peaks in the XPS spectra confirm the full sulfurization of the material in the H_2S atmosphere with the optimized conditions.

Indirect-to-direct band gap transition. Another characteristic of thin van-der-Waals bonded layers are the layer-dependent property changes. A special TMD material characteristic is evolution of its PL for monolayers due to the indirect-to-direct bandgap transition. We applied the high temperature recipe with the pure H_2S gas to different thicknesses of TM/TMO. The thinner Mo/MoO_3 layers showed higher PL after the sulfurization process. This evolving PL indicates the efficiency of the sulfurization process and can be used as an indicator for further process optimization. Considering the fact that an initial Mo thickness of 0.5 nm corresponds to 3 monolayers, the PL could be further enhanced by using double- or monolayer structures.

Conclusions

In this work we investigated the sulfurization of thin transition-metal layers in H_2S and H_2S/H_2 mixtures. The reaction kinetics in TMO were determined by the H_2S partial pressure, whereas the sulfurization of metallic TM depends on the hydrogen content as well, since the presence of hydrogen slows down the sulfurization reaction in metallic TMs. The best TMD layers were obtained in pure H_2S ambient. The full sulfurization of metallic TM requires high temperatures of 800 °C resulting in higher film expansion than in the case of sulfurizing TMOs, which can be sulfurized at a lower temperature of 600 °C.

Gaseous byproducts of the sulfurization reaction escape in between the planes and affect their orientation during the ongoing sulfurization reaction. Reaction products such as H_2O could cause delamination of the MoS_2 films at the interface due to byproduct accumulation. Reducing substrates in combination with permeable thin layers could decrease film delamination.

After full sulfurization, the films recrystallize and their orientation is found to depend on the surface roughness of the underlying substrate. Hence, flat substrates such as native oxides or thermal dry oxides result in horizontal basal plane arrangement, whereas rougher substrates such as very thick wet oxide induce rather random basal plane orientation.

The high temperature process resulted in the formation of grains of a few 100 nm^2 and showed evolving PL on the ultra-thin films. This work shows that the sulfurization chemistry and process temperature need to be carefully adjusted for the material to be sulfurized and that the interface roughness plays an important role for the assembly of the basal planes. Further work, in view of a successful very large scale integration, will have to concentrate on the increase of the lateral grain size to minimize defects and improve electrical properties.

Acknowledgements

The authors appreciate the funding by the Agency for Innovation by Science and Technology (IWT).

References

1 B. Radisavljevic, A. Radenovic, J. Brivio, V. Giacometti and A. Kis, *Nat. Nanotechnol.*, 2011, **6**, 147–150.
2 K. Alam and R. K. Lake, *IEEE Trans. Electron Devices*, 2012, **59**, 3250–3254.
3 R. Addou, S. McDonnell, D. Barrera, Z. Guo, A. Azcatl, J. Wang, H. Zhu, C. L. Hinkle, M. Quevedo-Lopez, H. N. Alshareef, L. Colombo, J. W. P. Hsu and R. M. Wallace, *ACS Nano*, 2015, **9**, 9124–9133.
4 R. Addou, L. Colombo and R. M. Wallace, *ACS Appl. Mater. Interfaces*, 2015, **7**, 11921–11929.
5 S. McDonnell, R. Addou, C. Buie, R. M. Wallace and C. L. Hinkle, *ACS Nano*, 2014, **8**, 2880–2888.
6 D. Sharma, M. Amani, A. Motayed, P. B. Shah, A. G. Birdwell, S. Najmaei, P. M. Ajayan, J. Lou, M. Dubey, Q. Li and A. V Davydov, *Nanotechnology*, 2014, **25**, 155702.
7 W. Zhang, J.-K. Huang, C.-H. Chen, Y.-H. Chang, Y.-J. Cheng and L.-J. Li, *Adv. Mater.*, 2013, **25**, 3456–3461.
8 K. K. H. Smithe, C. D. English, S. V. Suryavanshi and E. Pop, in 2015 73rd Annual Device Research Conference (DRC), IEEE, 2015, vol. 3087, pp. 239–240.
9 Y. Zhan, Z. Liu, S. Najmaei, P. M. Ajayan and J. Lou, *Small*, 2012, **8**, 966–971.
10 G. Plechinger, J. Mann, E. Preciado, D. Barroso, A. Nguyen, J. Eroms, C. Schüller, L. Bartels and T. Korn, *Semicond. Sci. Technol.*, 2014, **29**, 064008.
11 D. N. Nath, M. Lu, H. L. Chong, E. Lee, A. Arehart, W. Yiying and S. Rajan, Electron transport in large-area epitaxial MoS2, in *Device Research Conference (DRC)*, 2014 72nd Annual, pp. 89–90, 22–25 June 2014, DOI: 10.1109/DRC.2014.6872311.
12 H. Schmidt, S. Wang, L. Chu, M. Toh, R. Kumar, W. Zhao, A. H. Castro Neto, J. Martin, S. Adam, B. Özyilmaz and G. Eda, *Nano Lett.*, 2014, **14**, 1909–1913.
13 S. Ghosh, S. Najmaei, S. Kar, R. Vajtai, J. Lou, N. R. Pradhan, L. Balicas, P. M. Ajayan and S. Talapatra, *Phys. Rev. B: Condens. Matter Mater. Phys.*, 2014, **89**, 125422.

14 Y. Lee, J. Lee, H. Bark, I.-K. Oh, G. H. Ryu, Z. Lee, H. Kim, J. H. Cho, J.-H. Ahn and C. Lee, *Nanoscale*, 2014, **6**, 2821–2826.
15 J. M. Wilson, *Surf. Sci.*, 1975, **53**, 330–340.
16 Y. Shi, Y. Wan, R. Liu, B. Tu and D. Zhao, *J. Am. Chem. Soc.*, 2007, **129**, 9522–9531.
17 L. P. Hansen, E. Johnson, M. Brorson and S. Helveg, *J. Phys. Chem. C*, 2014, **118**, 22768–22773.
18 J. A. Miwa, M. Dendzik, S. S. Grønborg, M. Bianchi, J. V Lauritsen, P. Hofmann and S. Ulstrup, *ACS Nano*, 2015, **9**, 6502–6510.
19 D.-W. Lee, J. Lee, I. Y. Sohn, B.-Y. Kim, Y. M. Son, H. Bark, J. Jung, M. Choi, T. H. Kim, C. Lee and N.-E. Lee, *Nano Res.*, 2015, **8**, 2340–2350.
20 I. Song, C. Park, M. Hong, J. Baik, H. J. Shin and H. C. Choi, *Angew. Chem., Int. Ed.*, 2014, **53**, 1266–1269.
21 H. G. Füchtbauer, A. K. Tuxen, Z. Li, H. Topsøe, J. V. Lauritsen and F. Besenbacher, *Top. Catal.*, 2014, **57**, 207–214.
22 Y.-C. Lin, R. K. Ghosh, R. Addou, N. Lu, S. M. Eichfeld, H. Zhu, M.-Y. Li, X. Peng, M. J. Kim, L.-J. Li, R. M. Wallace, S. Datta and J. A. Robinson, *Nat. Commun.*, 2015, **6**, 7311.
23 R. Yue, A. T. Barton, H. Zhu, A. Azcatl, L. F. Pena, J. Wang, X. Peng, N. Lu, L. Cheng, R. Addou, S. Mcdonnell, L. Colombo, J. W. P. Hsu, J. Kim, M. J. Kim, R. M. Wallace and C. L. Hinkle, *ACS Nano*, 2015, **9**, 474–480.
24 B. Holländer, H. Heer, M. Wagener, H. Halling and S. Mantl, *Nucl. Instrum. Methods Phys. Res., Sect. B*, 2000, **161–163**, 227–230.
25 N. H. Turner and A. M. Single, *Surf. Interface Anal.*, 1990, **15**, 215–222.
26 J.-G. Choi and L. T. Thompson, *Appl. Surf. Sci.*, 1996, **93**, 143–149.
27 M. a Albiter, R. Huirache-Acuña, F. Paraguay-Delgado, J. L. Rico and G. Alonso-Nuñez, *Nanotechnology*, 2006, **17**, 3473–3481.
28 B. Schönfeld, J. J. Huang and S. C. Moss, *Acta Crystallogr., Sect. B: Struct. Sci.*, 1983, **39**, 404–407.
29 A. V. Chichagov, *Kristallografiya*, 1990, **35**, 610–616.
30 A. Gurarslan, Y. Yu, L. Su, Y. Yu, F. Suarez, S. Yao, Y. Zhu, M. Ozturk, Y. Zhang and L. Cao, *ACS Nano*, 2014, **8**, 11522–11528.
31 N. Scheuschner, O. Ochedowski, A.-M. Kaulitz, R. Gillen, M. Schleberger and J. Maultzsch, *Phys. Rev. B: Condens. Matter Mater. Phys.*, 2014, **89**, 125406.
32 Q. Ji, Y. Y. Zhang, T. Gao, D. Ma, M. Liu, Y. Chen, X. Qiao, P.-H. Tan, M. Kan, J. Feng, Q. Sun and Z. Liu, *Nano Lett.*, 2013, **13**, 1–15.
33 A. Splendiani, L. Sun, Y. Zhang, T. Li, J. Kim, C.-Y. Chim, G. Galli and F. Wang, *Nano Lett.*, 2010, **10**, 1271–1275.
34 K. F. Mak, K. He, C. Lee, G. H. Lee, J. Hone, T. F. Heinz and J. Shan, *Nat. Mater.*, 2013, **12**, 207–211.
35 K.-K. Liu, W. Zhang, Y. Lee, Y.-C. Lin, M.-T. Chang, C.-Y. Su, C.-S. Chang, H. Li, Y. Shi, H. Zhang, C.-S. Lai and L.-J. Li, *Nano Lett.*, 2012, **12**, 1538–1544.
36 X. Lee, X. Li, X. Zang, M. Zhu, Y. He, K. Wang, D. Xie and H. Zhu, *Nanoscale*, 2015, 8398–8404.
37 A. P. S. Gaur, S. Sahoo, M. Ahmadi, S. P. Dash, M. J. F. Guinel and R. S. Katiyar, *Nano Lett.*, 2014, **14**, 4314–4321.
38 T. Bakos, S. N. Rashkeev and S. T. Pantelides, *Phys. Rev. Lett.*, 2002, **88**, 055508.
39 S. Kostinski, R. Pandey, S. Gowtham, U. Pernisz and A. Kostinski, *IEEE Electron Device Lett.*, 2012, **33**, 863–865.
40 D. Kong, H. Wang, J. J. Cha, M. Pasta, K. J. Koski, J. Yao and Y. Cui, *Nano Lett.*, 2013, **13**, 1341–1347.
41 J. Lee, P. Dak, Y. Lee, H. Park, W. Choi, M. A. Alam and S. Kim, *Sci. Rep.*, 2014, **4**, 7352.
42 D. Sercombe, S. Schwarz, O. Del Pozo-Zamudio, F. Liu, B. J. Robinson, E. A. Chekhovich, I. I. Tartakovskii, O. Kolosov and A. I. Tartakovskii, *Sci. Rep.*, 2013, **3**, 3489.
43 N. Choudhary, J. Park, J. Y. Hwang and W. Choi, *ACS Appl. Mater. Interfaces*, 2014, **6**, 21215–21222.
44 M. Maeda, K. Nakamura and T. Ohkubo, *J. Mater. Sci.*, 1989, **24**, 2120–2126.
45 P. O. Hahn, *J. Appl. Phys.*, 1981, **52**, 4122.
46 J. Zhang, H. Yu, W. Chen, X. Tian, D. Liu, M. Cheng, G. Xie, W. Yang, R. Yang, X. Bai, D. Shi and G. Zhang, *ACS Nano*, 2014, **8**, 6024–6030.
47 Z. Jin, S. Shin, D. H. Kwon, S.-J. Han and Y.-S. Min, *Nanoscale*, 2014, **6**, 14453–14458.
48 E. Minni and F. Werfel, *Surf. Interface Anal.*, 1988, **12**, 385–390.
49 R. Kappera, D. Voiry, S. E. Yalcin, B. Branch, G. Gupta, A. D. Mohite and M. Chhowalla, *Nat. Mater.*, 2014, **13**, 1128–1134.
50 Y. Lu, X. Yao, J. Yin, G. Peng, P. Cui and X. Xu, *RSC Adv.*, 2015, **5**, 7938–7943.
51 L. Jiang, S. Zhang, S. A. Kulinich, X. Song, J. Zhu, X. Wang and H. Zeng, *Mater. Res. Lett.*, 2015, **3**, 177–183.

